Volume 1 | Number 1 | Jan 2013 | Pages 1–100

RSC Advances

www.rsc.org/advances

ROYAL SOCIETY OF CHEMISTRY

ROYAL SOCIETY OF CHEMISTRY

www.rsc.org/advances

RSC Advances

RSC Advances

ARTICLE

Influence of phosphate precursor on the structure, crystallization behaviour and bioactivity of sol-gel derived 45S5 bioglass

Nisha Shankhwar,[a] G. P. Kothiyal[b] and A. Srinivasan[a]

Obtaining bioglass composition 45S5® in completely amorphous form without crystalline inclusion by sol-gel route has remained a challenge so far. Here, we demonstrate that with appropriate phosphate precursor and by controlling the polymerization and gelation reactions by adjusting the pH of the reactants, one can overcome this challenge. As-synthesized glass was heat treated to understand the devitrification behaviour of the sol-gel derived glass and to obtain bioglass-ceramics. As-synthesized and heat treated glass were characterized using powder X-ray diffraction, transmission electron microscope, differential scanning calorimeter and differential thermal analyzer. For assessing the *in vitro* bioactivity of sol-gel derived glass and glass-ceramic powders, we tested the apatite forming ability on their surface upon immersion in simulated body fluid. Properties of sol-derived 45S5 glass are then compared with the bulk counterpart obtained by conventional melt quenching method. This study reveals a procedure to prepare completely amorphous sol-gel derived 45S5 glass which can be used as a bioactive material for bone implant, tooth coating, bone tissue engineering and drug delivery applications.

Introduction

Bioactive glasses are used as bone regenerative materials. These biomaterials develop a bone-like surface layer of hydroxyapatite (HA) under physiological conditions which provides them a strong bonding with tissues [1–4,5,6]. Hench reported the first bioactive glass composition bioglass 45S5, which is a silica-based melt-derived glass with a composition of $45SiO_2.24.5Na_2O.24.5CaO.6P_2O_5$ (in wt%) (or $46.1SiO_2.26.9CaO.24.4Na_2O.2.5P_2O_5$ in mol%) [2]. Though many other bioactive glass and glass-ceramic compositions have been developed in bulk form by melt-quenching method [5], the 45S5 composition is considered as a prototype bioglass due to its excellent bioactivity [2]. However, the brittle nature of bioglass has considerably hindered its application due to its poor load bearing ability [3]. Nanoporous bioactive glass, such as the one obtained from sol-gel process has several advantages such as high purity, better homogeneity at comparatively low fabrication temperature [6,7], higher mechanical strength [8], and better binding with tissue [9].

Sol-gel is a wet chemical process involving the formation of a sol by hydrolysis of precursors of the components and subsequent gelation of the sol [10,11]. The exact mechanism behind the silica sol–gel process is not yet well understood and is a subject of considerable debate. The sol-gel process is not a stepwise reaction as the hydrolysis and condensation happen almost simultaneously. Catteaux *et. al* [12], Adams *et. al* [13], Hamidreza *et. al* [14], Pourhashem *et. al* [15] attempted to prepare sol-gel glasses with compositions close to bioglass 45S5, but the end products invariably contained crystalline inclusions. Though SiO_2-CaO-P_2O_5 compositions containing lower Na_2O content have been obtained in completely amorphous form [16], fully amorphous sol-gel derived 45S5 glass composition is still elusive. Literature shows that tetra ethylorthosilicate (TEOS, $SiC_8H_{20}O_4$) is generally used as the precursor for silica in sol-gel synthesis of silicate glasses. Similarly, nitrates of calcium and sodium are used as precursors for CaO and Na_2O, respectively [17,18,12]. On the other hand, a wide variety of phosphate precursor such as triethylphosphate (TEP) [19,20,12], Phosphoric acid, P_2O_5 [18], triethyl phosphite (($C_2H_5O)_3P$) [20] have been used. It is to be noted that the monophosphate unit $(PO_4)^{3-}$ in the phosphate precursor provides good glass former ability but at the same time it is a poor gel former. Attempts to prepare several quaternary bioactive glass compositions by Siqueira *et. al* [18] and Padilla *et. al* [17] by varying the phosphate precursors resulted in semi-amorphous end products. Vallet-Regí, *et. al* [21] pointed out that the challenge lies in optimization and control of nitrates and phosphate precursors used in the sol-gel synthesis of bioglass.

We realized that the challenge lies in identifying suitable phosphate precursor and controlling the hydrolysis and gelation reactions. Here, we report a procedure for obtaining completely amorphous bioglass with composition close to

[a.] *Department of Physics, Indian Institute of Technology Guwahati, Guwahati 781039, India.*
[b.] *Glass and Advanced Ceramics Division, Bhabha Atomic Research Centre, Mumbai - 400085, India.*

bioglass 45S5 by sol-gel route by taking these points into account. The devitrification characteristics and in vitro bioactivity of sol-gel derived 45S5 glass was then evaluated. Finally, the properties of the sol-gel derived glass and the glass-ceramic have been compared with bulk melt quenched counterparts to showcase the potential of the former for bone regeneration applications.

Experimental Section

Materials

Tetraethyl orthosilicate (TEOS, $\geq$ 99%, Sigma-Aldrich) was used as the precursor for the glass former, *viz.,* silica. Calcium nitrate tetrahydrate ($Ca(NO_3)_2.4H_2O$, 99%, Lobachemie Pvt. Ltd., India) and sodium nitrate ($NaNO_3$, 99%, Merck Specialities Pvt. Ltd., India) were used as precursors for network modifiers CaO and Na_2O. Three phosphate precursors, viz., phosphorous pentaoxide (P_2O_5, 98%, Merck Specialities Pvt. Ltd., India), phosphoric acid (H_3PO_4, 88%, G.S. Chemicals, India) and di-ammonium hydrogen orthophosphate (($NH_4)_2HPO_4$, 99%, Lobachemie Pvt. Ltd., India) were used in our search to find the suitable precursor. Nitric acid (HNO_3, GR grade, Merck Specialities Pvt. Ltd., India) was used as catalyst. Deionized water was used as solvent.

Preparation

The reactants were taken in proportions required to obtain a final product with the 45S5 composition, *viz.,* 45 wt% SiO_2, 24.5 wt% Na_2O, 24.5 wt% CaO, and 6 wt% P_2O_5. 1 mol L^{-1} HNO_3 was used as catalyst to maintain a pH of 1~2 required to initiate hydrolysis at room temperature since TEOS by itself is not very sensitive to hydrolysis. Condensation reaction followed at room temperature at a slightly higher pH value. Same sol-gel procedure was adopted for the three different phosphate precursors in order to understand the effect of the phosphate precursor under controlled aqueous acidic environment. The procedure adopted is depicted in the flow chart shown in Fig. 1. First, 1.454 g TEOS dissolved in 10 ml of deionized water was added to 1 M HNO_3, and the mixture was allowed to react for 1 h for the hydrolysis of the precursor through continuous stirring. 0.897 g $Ca(NO_3)_2.4H_2O$ and 0.123 g $NaNO_3$ dissolved in 10 ml deionized water separately, were then added drop-wise to the TEOS solution and stirred for 1 h to obtain a transparent sol. Precursors in aqueous form facilitate hydrolysis reaction which minimize the chances of precipitation. Then, appropriate amount of phosphate precursor (say, P_2O_5 or H_3PO_4 or ($NH_4)_2HPO_4$)) solution was added drop-wise to the sol, maintaining a pH of 2~3. Finally, the as-mixed sol was stirred for 24 h to form a gel. As-prepared gel was aged for 3 days at ambient conditions and freeze dried at −40 °C. As-dried powder was heat treated at 70 °C for 3 days to eliminate nitrates and other unreacted substances. The last step represents thermal stabilization of the powders in which residual nitrates and other unreacted substances are removed in gaseous form leaving behind a highly porous and
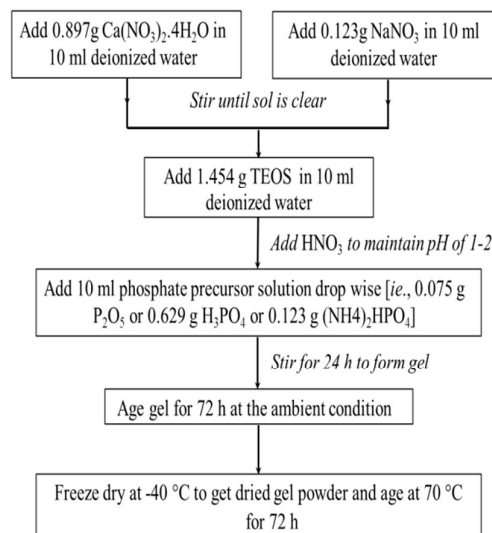
Fig. 1. Flowchart describing the steps involved in preparing 45S5 glass by sol-gel route.

gelatinous powder. Absence of characteristic N-O bands in the Fourier Transform Infra-red spectrum (not shown here) confirmed the elimination of nitrates. Dried powders were designated as $BG\_P_2O_5$, $BG\_H_3PO_4$ and $BG\_(NH_4)_2HPO_4$ based on the phosphate precursor used in the synthesis.

Characterization

X-ray diffraction (XRD) patterns of glass and glass-ceramic powders were recorded using Rigaku TTRAX III powder X-ray diffractometer operating at a power of 9.5 kW (50 kV, 190 mA) with Cu K_α (λ = 1.541 Å) radiation. Diffraction patterns were collected in the 2θ range of 10° to 70° in steps of 0.03° with 3s sampling time per step. The data base from the International Centre for Diffraction Data (ICDD) was used for identifying sodium calcium silicate ($Na_2Ca_2Si_3O_9$, PDF # 78-0364), wollastonite ($CaSiO_3$, PDF # 84-0655) and calcium phosphate ($Ca_4P_6O_{19}$, PDF# 15-0177) crystalline phases present in the XRD patterns of heat treated glass. Transmission electron microscopy (Tecnai TF20 TEM operated at 200 kV) was used to confirm the amorphous nature of the glass sample. High resolution TEM (HRTEM) images were taken at a direct magnification of 100000X. Differential scanning calorimeter (DSC, NETZSCH STA) and Differential thermal analyser (DTA, Hitachi STA7200) were used for thermal analysis of the glass samples. DSC curves were recorded at a constant heating rate of 20 Kminute^{-1} from ambient temperature to 900 °C after baseline subtraction. DTA curves recorded at 5, 10, 15 and 20 Kminute^{-1} were used to estimate the activation energy associated with the glass transition by employing the Kissinger equation [22]. Glass samples were heat treated above the glass transition temperature (between 650 °C and 850 °C) for 1h each to form glass-ceramics. In vitro bioactivity of the glass and glass-

ceramic was evaluated by immersing samples in freshly prepared simulated body fluid (SBF) [23] maintained at 37 °C and a pH of 7.40. Samples were removed at periodic intervals, lightly washed with deionized water, benignly dried and examined with grazing incidence X-ray diffractometer (GI-XRD) and field emission electron microscope (Zeiss Sigma) to confirm and quantify the growth of HA layer on the surface of SBF treated sample. The surface chemical analysis was carried out by energy dispersive X-ray spectroscopy (EDS) analysis. pH variation during *in vitro* test was monitored with a calibrated pH meter (EUTECH pH Tutor).

Results and Discussion

XRD patterns of the dried gel powders prepared using different phosphate precursors are shown in Fig. 2(a-c). In an earlier report, XRD pattern of SiO_2–CaO–P_2O_5 glass gel powders exhibited the presence of crystalline phosphate phases [18]. Moreover, attempts to include 5% to 90% of P_2O_5 in SiO_2–CaO–P_2O_5 led to partially crystallized gel powders [17]. When H_3PO_4 is used as phosphate precursor, sudden precipitation of gel takes place in the presence HNO_3 catalyst, leading to the crystallization of $Na_2Ca_2Si_3O_9$ as the major phase and $CaSiO_3$ as a minor phase as shown in Fig. 2(b).

The microstructure of the specimen obtained by sol-gel process depends on the hydrolysis and condensation reactions. A number of conditions can influence the hydrolysis and condensation reactions. Of these, the most pertinent ones are water-to-alkoxide ratio, type and amount of catalyst, type of organic group attached to the silicon atom and solvent effects [24].
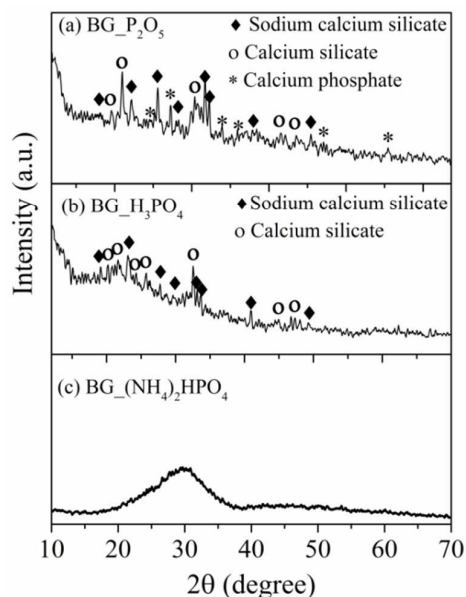
Sol-gel is highly pH sensitive reaction and can be processed under basic and acidic environments. Several pH-dependent rate profiles have been reported for the hydrolysis and condensation reactions, where it has been found that reaction rates are largely dependent on pH [7]. For instance, in acid catalyzed reaction, hydrolysis occurs at a higher rate, while condensation occurs at a slower rate. Moreover, in base catalyzed reaction, an inverse behaviour has been noticed between the rates of the two reactions [7, 24–26]. It is this inverse relationship between the rates of the hydrolysis and condensation reactions that must be taken into account in controlling the kinetics of the reaction and hence controlling the ultimate network structure. To create a desirable amorphous glassy network through the sol–gel process, the sol must undergo a rapid hydrolysis followed by a slower gelation process. With this understanding, we proceeded to test the phosphate precursor $(NH_4)_2HPO_4$. This phosphate precursor is basic in pH. Hence, after complete hydrolysis at an acidic pH of 1~2, $(NH_4)_2HPO_4$ increases the pH of the mixture towards basic region. The higher pH influences the kinetics of the reaction and results in slower gelation. Slower gelation results in less number of untreated constituents which ultimately precipitate as crystalline phases. Such pH control of the reactions with the use of $(NH_4)_2HPO_4$ can thus induce rapid hydrolysis and slower gelation and hence an amorphous gel product. Fully amorphous XRD pattern of BG_$(NH_4)_2HPO_4$ gel powder is depicted in Fig. 2(c) which confirms the above reasoning and illustrates the role of $(NH_4)_2HPO_4$ in obtaining a fully amorphous 45S5 glass by sol-gel process.

In order to confirm the amorphous nature of BG_$(NH_4)_2HPO_4$ down to atomic length scales, high resolution transmission electron microscope (HRTEM) images were taken. HRTEM image shown in Fig. 3(a) confirms the complete amorphous structure of BG_$(NH_4)_2HPO_4$ as no lattice fringes depicting crystalline order could be seen down to a few nm scale.

Fig.2. Room temperature XRD patterns of sol-gel derived powders using (a) P_2O_5, (b) H_3PO_4 and (c) $(NH_4)_2HPO_4$ phosphate precursors.
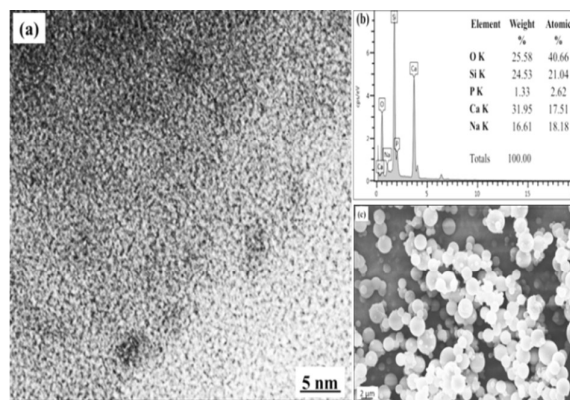
Fig. 3. (a) HRTEM image, (b) EDS spectrum with overall elemental composition map, and (c) FESEM image of BG_$(NH_4)_2HPO_4$.

Fig. 3(b) shows the EDS spectra and the overall concentration of the elements present in the specimen, It can be seen that the measured elemental compositions are Si (21.04 at.%), Ca (17.51 at.%), Na (18.18 at.%), P (2.62 at.%) and O (40.66 at.%) against the nominal composition of 45S5, *viz.,* Si (21.55 at.%), Ca (18.22 at.%), Na (18.10 at.%), P (2.1 at.%) and O (40.03 at.%). The close agreement with the measured and nominal elemental compositions shows that the specimen has a composition very close to 45S5. Fig. 3(c) shows the low resolution FESEM image of the 45S5 gel dried powders showing nearly spherical agglomerated amorphous particles.

Having successfully prepared fully amorphous glass with composition very close to bioglass 45S5 by sol-gel route, we proceeded to characterize the glass. Glass transition temperature (T_g) is the most important parameter for a glass. Fig. 4 shows the DSC curve of BG_$(NH_4)_2HPO_4$ recorded at a constant heating rate of 20 K minute^{-1}, illustrating an endothermic baseline shift beginning at 661 °C, and an exotherm with onset at 840 °C and peak at 896 °C. The endothermic baseline shift signifies the supercooled liquid to liquid (glass) transition. The onset temperature of the transition is identified as T_g [28]. The exotherm corresponds to the crystallization of the bone mineral phase sodium calcium silicate. Bretcanu *et al.* [28] obtained crystallization temperature (T_g) (onset) at 549 °C and T_c (peak) of 676 °C for melt quenched 45S5 glass powder from DTA curve recorded at the same heating rate. Massera et al. [29] reported T_g and T_c of melt quenched 45S5 glass powder particles of size < 45 μm heated at 15 Kminute^{-1} to be 552 °C and 715 °C, respectively. They also observed that T_c increased considerably for coarser (300 – 500 μm) powders. The dependence of the characteristic temperatures on the particle size of melt quenched 45S5 glass makes it difficult to make a direct comparison of the characteristic temperatures of the sol-gel and melt quenched glasses. However, the large difference between T_c and T_g observed in the case of the sol-gel glass powders is obvious from the above comparison.

A kinetically controlled reaction temperature such as T_g shifts with heating rate. Once the data on T_g at different heating rates are available, the activation energy which is a measure of the inhibition to the reaction could be estimated. Kissinger's equation [22] given below is an Arrhenius equation from which the activation energy could be determined.

$$\frac{d\left[\ln\dfrac{\phi}{T_g^2}\right]}{d\left[\dfrac{1}{T_g}\right]} = -\frac{E_K}{R} \qquad (1)$$

where ϕ is the heating rate, E_K is the activation energy for glass transition obtained from the Kissinger equation and R is the universal gas constant.

Fig. 5 shows the DTA curves of BG_$(NH_4)_2HPO_4$ recorded at constant heating rates of 5 to 20 Kminute^{-1}, illustrating the corresponding shift (624 – 661 °C) in T_g with heating rate.
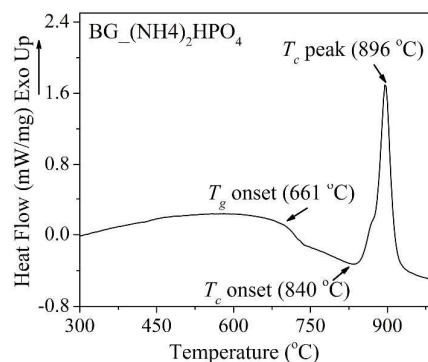
Fig. 4. DSC curve of BG_$(NH_4)_2HPO_4$ recorded at ϕ = 20 K minute^{-1}, showing glass transition and crystallization temperatures.

Inset in Fig. 5 shows the Arrhenius plot corresponding to Eq. (1) and the least squares fit to data to extract E_K. E_K (= 250 kJ mol^{-1}) obtained can be compared with the values of 316 kJ mol^{-1} [28] reported for melt quenched 45S5 glass powder, which indicates that the sol gel derived glass has relatively better thermal stability. Based on the DTA curves depicted in Fig. 5, BG_$(NH_4)_2HPO_4$ was heat treated above its T_g at three different temperature, *viz.,* 650, 750 and 850 °C for 1 h each to induce crystallization and form glass-ceramics. Since we have a fully amorphous glass in BG_$(NH_4)_2HPO_4$, this study will also help us in understanding the devitrification behaviour of the 45S5 sol-ge derived glass. Fig. 6 shows the XRD patterns of heat treated BG_$(NH_4)_2HPO_4$ indicating the presence of sodium calcium silicate ($Na_2Ca_2Si_3O_9$, PDF # 78-0364). It is clear from Fig. 6 that $Na_2Ca_2Si_3O_9$ is the only phase crystallizing in the glass heat treated up to 850 °C. Fully developed Bragg peaks and the flat baseline shows that the crystallization of this phase is nearly complete after heat treatment at 850 °C. Reports in the literature show that heat treatment above 600 °C results in the crystallization of $Na_2Ca_2Si_3O_9$ as the main crystalline phase in sol-gel derived Na_2O–CaO–$2SiO_2$ system [13,28,30].
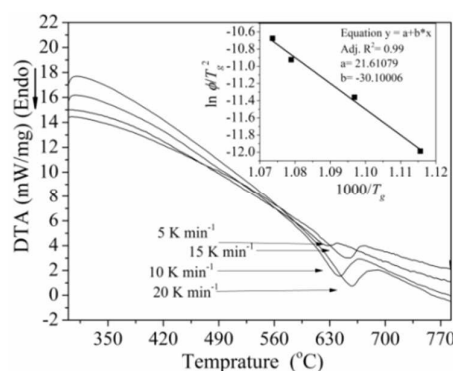
Fig. 5. DTA curves recorded at 5, 10, 15, 20 K minute^{-1} near T_g of BG_$(NH_4)_2HPO_4$. Inset shows the Kissinger's plot and the least squares fit to extract E_K.
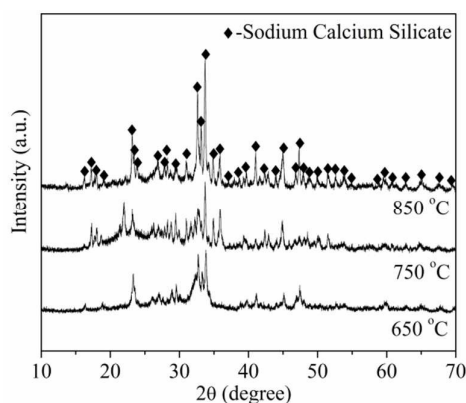
Fig.6. Room temperature XRD patterns of BG_(NH4)$_2$HPO$_4$ heat treated at different temperatures.

Average crystallite size (d_{av}) and microstrain (ε) of Na$_2$Ca$_2$Si$_3$O$_9$ phase in BG_(NH$_4$)$_2$HPO$_4$ heat treated at different temperatures has been estimated from the data in Fig. 6 using the Williamson - Hall relation [31],

$$\beta\cos\theta = K\lambda/d_{av} + 4\varepsilon\sin\theta \qquad (2)$$

where β is the integral breadth (full width at half maximum) of diffraction peak, λ is wavelength, K is the Schérrer constant (which is 0.89 for nearly spherical particles and θ is the Bragg angle. If the second term is neglected, Eq. (2) reduces to the Schérrer relation. d_{av} of Na$_2$Ca$_2$Si$_3$O$_9$ increases almost linearly with heat treatment temperature, *i.e.*, from 29 ± 0.05 nm (ε = 23 × 10^{-5}), 32 ± 0.05 nm (ε = 37 × 10^{-5}) nm and 38 ± 0.05 nm (ε = 45 × 10^{-5}) for 650, 750 and 850 °C respectively. Increase in crystallite size due to growth of the crystallites with increase in heat treatment temperature is expected. The continuous increase in ε with increasing temperature is a consequence of the rapid growth of the nanocrystallites within the confined space in the glassy matrix.

The rate of formation of HA surface layer is a measure of bioactivity of the specimen placed in physiological environment. HA forming ability is considered to be a critical factor in facilitating the chemical fixation of biomaterials to bone tissue, and ultimately the in vivo success of the bone grafting material [17,23,31,32]. BG_(NH$_4$)$_2$HPO$_4$ and glass-ceramics obtained by heated treatment of BG_(NH$_4$)$_2$HPO$_4$ at 850 °C for 1 h were chosen for *in vitro* bioactivity test. Powders of glass and glass-ceramic specimen were cold compacted into pellets of 10 mm diameter in a hydraulic press under a pressure of 6 Ton/cm^2 and the pellets were gently polished to yield a smooth surface. *In vitro* bioactivity test was carried out by soaking both BG_(NH$_4$)$_2$HPO$_4$ glass and the glass ceramic pellets in simulated body fluid (SBF). SBF was prepared according to the procedure proposed by Kokubo *et. al* [23]. Temperature of the solution was maintained at 37 °C and its initial pH was adjusted at 7.40 by adding 50 mM (tris-hydroxymethyl)-aminomethane and 45 mM HCl to simulate the physiological environment *in vitro*. Pellets immersed in SBF

were taken out after 1, 3, 5, 10 and 15 days, gently washed in distilled water and benignly dried for examination. The mechanism of HA-like phase formation on the silica based materials in SBF solution can be explained in terms of a chemical reaction taking place between the glass ceramic materials and the solution [23,33].

When bioactive glass/glass-ceramic comes in contact with SBF, a partial dissolution occurs producing an ionic exchange of Ca^{2+} for 2H$^+$ within the material network leading to the formation of silanol groups on the surface of the glass/glass-ceramics. Later, there is a partial dissolution of amorphous silica as SiO$_3$$^{2-}$. This enhances the creation of crystallization nuclei for the Ca–P phase. Structural changes on the surface of the glass/glass-ceramics samples treated in SBF were analyzed using GI-XRD (Fig. 7 and Fig. 8). pH of SBF was also recorded as function of immersion time (Fig. 9). Appearance of crystalline peaks in the GI-XRD patterns of glass samples immersed in SBF for a day or more, confirms the formation of a crystalline layer on the surface of the glass. On soaking in SBF for 3 days, prominent peaks appear at 2θ values of ~26° and ~32°. These peaks correspond to (002) and (211) reflections of hydroxyapatite (HA) crystallites (PDF # 74-0565). Minor peaks of wollastonite (Calcium silicate) phase were also observed as an intermediate phase during the immersion period. Fig. 7 and 8 show the growth of HA on the surface of glass and glass-ceramic pellets with immersion time. Average size (d_{av}) of HA crystallized was estimated from the (002) reflection at 25.88° peak using the Schérrer`s relation (first term in Eq. 2, d_{av} increases from 17 ± 0.5 nm to 41 ± 0.6 nm in glass and from 28 ± 0.5 nm to 52 ± 0.6 nm in glass ceramic, respectively, after immersion for 3 days to 15 days in SBF.

Fig. 9 shows that the trends in HA crystallite growth on both glass and glass ceramic with immersion time is almost similar. A rapid increase in crystallite size up to 5 days of immersion followed by a slower and linear increase thereafter is seen for both the glass and glass-ceramic samples.
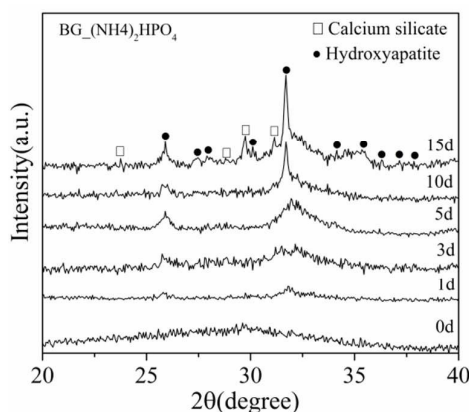
Fig.7. GI-XRD patterns of BG_(NH4)$_2$HPO$_4$ showing the nucleation and growth of HA surface layer as a function of immersion time in SBF.
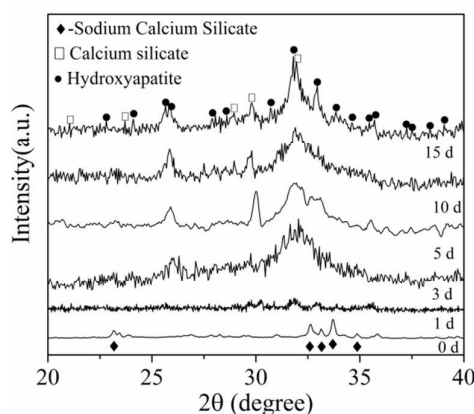
Fig. 8. GI-XRD patterns of glass ceramic derived by heat treating BG_(NH4)$_2$HPO$_4$ at 850 °C for 1 h. as a function of immersion time in SBF.

In the case of the glass-ceramic sample, consistent higher HA crystallite size suggests an enhanced growth of HA layer on its surface as compared to the glass.

The slight increase in the HA crystallite size on ceramic is due to the presence of bone mineral phases at its surface. This confirms the strong bioactive character of the samples which is primarily due to the large amounts of bone mineral phase present in the sample.

pH of SBF solution plays a crucial role in deciding the bioactive nature of the specimen. pH variation was recorded to understand the ion exchange mechanism between glass/glass-ceramics surface and SBF as a function of immersion time (*c.f.* Fig. 10). Two aspects of pH variation need a careful observation *viz.,* change in magnitude of pH value and rate of change of pH. Mechanism of HA formation in bioactive silica-based ceramic materials can be described in terms of pH variation of SBF as follows: During early stage of immersion, the reaction is initiated through exchange of H_3O^+ ions from SBF with cations such as Na^+, Ca^{2+} in the sample.
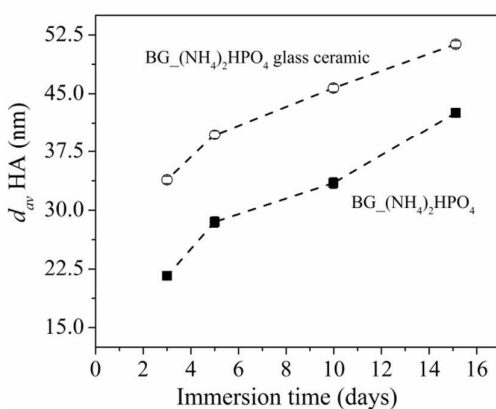
Fig. 9. Average crystallite size of HA surface layer on sol-gel derived glass (filled square) and glass ceramic (open circle) after immersion in SBF.
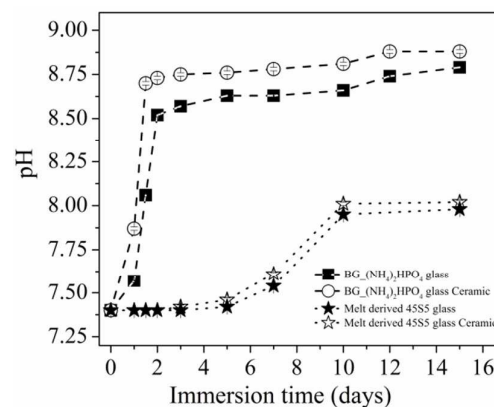
Fig. 10. Variation of pH of BG_(NH4)$_2$HPO$_4$ glass (filled squares) and glass ceramic (open squares) as a function of immersion time in SBF. Data on melt derived 45S5 glass (filled stars) and glass ceramic (open stars) are also shown for comparison.

Growth profiles of HA amorphous sol-gel and melt derived 45S5 glass/glass ceramic are different. Because of higher surface reactivity of sol-gel derived glass/glass ceramic, a slight increase in pH is observed as early as after 12 h of immersion. Though H_3O+ ions do not influence the pH of the SBF much (Fig. 10), they initiate the necessary hydrolysis reaction. This ion exchange reaction results in the formation of a hydrated silica gel layer.

This layer is abundant in silanol (Si-OH) groups and provides favourable sites for the calcium phosphate nucleation. Further, water molecules in the SBF react with the Si-O-Si bond to form additional Si-OH groups which induce HA nucleation. The results show that the reaction is faster during the early stage of immersion (3 days) in the case of the sol-gel derived samples than in the melt-derived counterparts. Sol-gel derived amorphous and crystalline specimen show faster pH variation whereas no pH variation was observed in case of melt derived specimen in early days of immersion. This is due to the higher roughness of the sol-gel glass/glass-ceramic surface, which facilitates the ion exchange mechanism leading to higher nucleation on the surface and hence rapid formation of HA on the surface.

Preferential growth of HA at different sites can be observed from FESEM micrographs shown in Fig. 11. Also, the glass ceramic specimen contains calcium-rich phase (sodium calcium silicate) on the surface of the gel-derived 45S5 which releases of Na^+, Ca^{2+} ions and accelerates HA nucleation by increasing the ionic activity in the fluid and promotes calcium phosphate nucleation on the surface of sample and rapid increase in pH of SBF. High dissolution rate and chemical degradation of sodium calcium phosphate on ceramic surface has been found to promote nucleation and growth of HA layer. Further, this higher pH of the SBF solution affects the interfacial reaction kinetics and promotes self-nucleation of HA. Eventually, the surface of the gel-derived 45S5 gets covered with fine HA as can be seen in micrographs (Fig. 11) at pH value 8.87 after 15 days of immersion. This study shows that BG_(NH$_4$)$_2$HPO$_4$ heat

RSC Advances

treated at 850 °C for 1 h induces larger and faster ion exchange with SBF, leading to rapid nucleation and growth of HA layer at the surface. However, the $BG\_(NH_4)_2HPO_4$ sample shows a lower pH (8.78) due to the time taken for initiation of ion exchange mechanism. Hamidreza *et. al* [34] suggested that bioactivity is more strongly related to the combination of crystallinity and surface texture of specimen rather than on a single variable such as crystallinity alone.

The results presented herein demonstrate that the glass-ceramic derived from $BG\_(NH_4)_2HPO_4$ has better bioactivity, as indicated by the pH-time profile to form HA and dissolution rate of sodium calcium silicate, than its melt derived counterpart.

FESEM micrographs (Fig. 11) of the $BG\_(NH_4)_2HPO_4$ provide visual evidence of gradual development of apatite on the surface of glass after immersion for various time periods in SBF. On immersion for a day, the surface shows agglomerated submicron sized HA particle. After 15 days of immersion, surface of sample is completely covered with HA layer. The EDS spectrum of the surface of sample immersed in SBF for 15 days is also shown in the figure.

Na and Cl presence is expected due to their presence in SBF. The value of Ca/P ratio of 1.66 obtained may be compared with the value of 1.67 of HA in human bone.
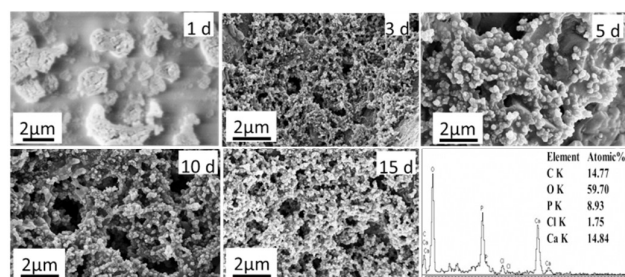
Fig. 11. FESEM micrographs of glass soaked in SBF for 15 days showing the growth of HA on the surface. EDS spectrum of 15 days immersed sample confirms Ca/P ratio of 1.66 at the surface.

Conclusions

We have successfully obtained fully amorphous glass with a composition very close to bioglass 45S5 by sol-gel route. Various phosphate precursors were used to check if an amorphous 45S5 phase could be obtained. Our attempts showed that with $(NH_4)_2HPO_4$ as the phosphate precursor, it is possible to obtain fully amorphous material with a composition close to bioglass 45S5. Sol-gel derived samples have been found to exhibit superior bioactivity as compared to the bulk melt derived counterparts. This study makes a significant impact on the debate on the relative merits of sol-gel and melt derived glass/glass ceramic. Since this methodology allows for production of materials with controlled stoichiometry and particle size, this methodology can be applied for production of biomaterials with potential application in biomedical field as bone implant material and

bone scaffolding application such as tooth coating, diagnosis, bone scaffolding, and drug delivery.

Acknowledgements

References

1   L. L. Hench, *Science*, 1980, **80,** 208.

2   L. L. Hench, *J. Mater. Sci. Mater. Med*., 2006, **17**, 967.

3   L. L. Hench, *J. Am. Ceram. Soc*., 1991, **74**, 1487.

4   L. L. Hench, *J. Am. Ceram. Soc*., 1998 **81,** 1705.

5   I. A. Silver, J. Deas and M. Erecin, 2001, 22.

6   J. V. Rau, R. Teghil, M. Fosca, a. De Bonis, I. Cacciotti, A. Bianco, V. R. Albertini, R. Caminiti and A. Ravaglioli, *Mater. Res. Bull.,* 2012, **47**, 1130.

7   R. W. Jones, "Fundamental Principles of Sol-gel Technology", IOM Communications Ltd. 1990.

8   S. Eqtesadi, A. Motealleh, P. Miranda, A. Pajares, A. Lemos and J. M. F. Ferreira, *J. Eur. Ceram. Soc.,* 2014, **34**, 107.

9   J. P. Fan, P. Kalia, L. Di Silvio and J. Huang, *Mater. Sci. Eng. C.* 2014, **36**, 206.

10 E. J. Nassar, K. J. Ciuffi, P. S. Calefi, L. A. Rocha, E. H. De Faria, M. L. A. e Silva, P. P. Luz, L. C. Bandeira, A. Cestari and C. N. Fernandes, Biomaterials Science and Engineering, 2001.

11 A. M. El-Kady, A. F. Ali and M. M. Farag, *Mater. Sci. Eng. C*, 2010, **30**, 120.

12 R. Catteaux, I. Grattepanche-Lebecq, F. Désanglois, F. Chai, J.-C. Hornez, S. Hampshire and C. Follet-Houttemane, *Chem. Eng. Res. Des.*, 2013, **91**, 2420.

13 E. R. Essien, L. A. Adams, R. O. Shaibu and A. Oki, *Biomed Sci Eng.,* 2013, **6**, 258.

14 H. Pirayesh and J. a. Nychka, J. Am. Ceram. Soc., 2013, 96, 1643–1650.

15 S. Pourhashem and A. Afshar, *Ceram. Int*., 2014, **40**, 993.

16 A. Lucas-Girot, F. Z. Mezahi, M. Mami, H. Oudadesse, A. Harabi and M. Le Floch, *J. Non. Cryst. Solids*, 2011, **357**, 3322.

17 S. Padilla, J. Román, a Carenas and M. Vallet-Regí, *Biomaterials*, 2005, **26**, 475.

18 R. L. Siqueira and E. D. Zanotto, *J. Mater. Sci. Mater. Med*., 2013, **24**, 365.

19 Q.-Z. Chen and G. A. Thouas, *Acta Biomater.,* 2011, **7,** 3616.

20 I. Cacciotti, M. Lombardi and L. Montanaro, *J Mater Sci: Mater Med*., 2012, **23,** 1849.

21 A. Rámila, F. Balas and M. Vallet-Regí, *Chem. Mater.*, 2002, **14**, 542.

22 A. Frączyk, *Techn. Sc.,* 2011, **14**.

23 T. Kokubo and H. Takadama, *Biomaterials*, 2006, **27**, 2907.

RSC Advances Accepted Manuscript

24 C. A. Milea and C. Bogatu, *Bull. Transilv. Univ. Brasov Eng. Sci.*, 2011, **4**, 59.

25 S. K. Young, Overview of Sol-Gel Science and Technology *Army research laboratory*, 2002.

26 E.D. Zanotto, *J. Non. Cryst. Solids,* 1992 **147** & **148** 820.

27 C. Brinker and G. Scherer, "Sol-gel science: the physics and chemistry of sol-gel processing", 1990.

28 O. Bretcanu, X. Chatzistavrou, K. Paraskevopoulos, R. Conradt, I. Thompson and A. Boccaccini, *J. Eur. Ceram. Soc.*, 2009, **29,** 3299.

29 J. Massera, S. Fagerlund, L. Hupa and Mikko Hupa, *J. Am. Ceram. Soc.,* 2012, **95,** 607.

30 D. C. Clupper and L. L. Hench, *J. Non. Cryst. Solids*, 2003, **318**, 43.

31 G. K. Williamson and W. H. Hall, *Acta Metall.,* 1953, **1,** 22.

32 O. H. Andersson and K. H. Karlsson, *J. Non. Cryst. Solids*, 1991, **129**, 145.

33 N. Shankhwar, G. P. Kothiyal and A. Srinivasan, *AIP Conf. Proc*., 2013, **1536**, 209.

34 C. Ohtsuki, T. Kokubo and T. Yamamuro, *J. Non. Cryst. Solids*, 1992, **143**, 84.
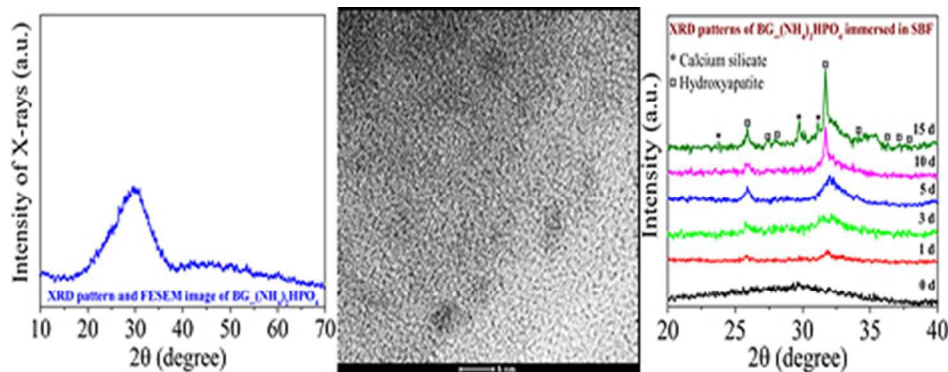
Sol-gel derived fully amorphous bioglass (BG_(NH$_4$)$_2$HPO$_4$) with composition close to bioglass 45S5 has been prepared and characterized.

79x39mm (150 x 150 DPI)